14èmes Journées de l'Hydrodynamique

18-19-20 novembre 2014

DGA Techniques hydrodynamiques
Chaussée du Vexin
27105 Val de Reuil

PREDICTION OF THE STRESS DISTRIBUTION ON A LEADING EDGE INFLATABLE KITE UNDER AERODYNAMIC LOAD

R LELOUP[1], G BLES[2], K RONCIN[2], J-B LEROUX[2], C JOCHUM[2], Y PARLIER[1]

[1]OCEA, Pépinière d'Entreprises COBAS, 1010 avenue de l'Europe, 33260 LA TESTE DE BUCH, richard.leloup@beyond-the-sea.com, www.beyond-the-sea.com/

[2]LBMS (EA 4325), ENSTA - Bretagne, 2 rue François Verny, 29806 BREST Cedex 9, France, guilhem.bles@ensta-bretagne.fr

Summary

The auxiliary propulsion of commercial ships requires huge kites for huge propulsive loads. Numerical tools must be implemented in order to evaluate the stress level within the kite fabric. In the present study, the kite fluid modelling is done using the 3D lifting line method. The load distribution is transferred to the structural modelling. The finite element analysis of the kite is based on shell elements for the fabric and beam elements for the laths. The stress distribution within the kite fabric is computed for the case of a *F-one Revolt* kite in a static flight case.

I – Introduction

Kites dedicated to auxiliary propulsion of commercial ships will be larger, more complex and more expensive than kites dedicated to kitesurfers. Such kites are currently studied by the beyond the sea® project. Therefore, numerical methods must be developed in order to compute stress distribution within the kite fabric. This data will be essential for the kite design especially for the fabric specifications. Various methods based on fluid-structure interaction were implemented in the literature to model soft sails like kites [1] or yacht sails [2,3].

Two main types of fluid structure interaction methods are used in the literature: the weak and strong coupling method. In a weak coupling method, aerodynamic and structural equations are solved independently. Two different software tools can be used: one is dedicated to solids structural analysis and the other one is dedicated to fluid analysis even if they were not initially developed to communicate together. The weak coupling approach is the most widely used for example for sail modelling by Chapin et al. [3], or for kite modelling by Breukel et al. [4] and Bosh et al. [1].

In the present study, the kite forces and velocities are defined according to the so-called zero-mass model [5,6]. Within this model, Newton's laws are applied considering only the

aerodynamic resultant and tethers tensions, since the mass of the kite is neglected. For a given true wind velocity and position of the kite within the wind window, the aerodynamic resultant, $\mathbf{F}_a$, balances the tethers tension, **T**, at any time and these two forces are aligned on the same axis $\mathbf{z}_{k0}$ shown in figure 3.

A weak coupling was chosen to allow a coupling between the structure analysis software ABAQUS and the 3D lifting line method presented in previous studies [5,6]. The advantage of using the 3D lifting line is that it takes into account the three-dimensional shape like the Vortex Lattice Method, but in addition it includes viscosity effects by a boundary layer calculation done with XFOIL. The kite geometry is based on the 3D scan of the *F-one Revolt* kite presented in previous studies [5,6]. It was used as the reference geometry at the beginning of the FSI process. The kite FEM model is presented in section II. The kite fabric was modelled using shell elements. The leading edge inflatable tube and inflatable battens were modelled using beam elements. The material characteristics were taken from experimental values. The load transfer between the 3D lifting line and the structure model is described in section III. The method used is similar to the one proposed by Breukels [4] and Bosch et al. [1]. Nevertheless, the profile load was transferred in a more precise manner. Moreover the three-dimensional flow effects which were not taken into account by Bosch at al. [1] were introduced thanks to the 3D lifting line. A similar mesh was used for the fluid and structure calculations to make the structure deformation transfer easy. The fluid structure interaction algorithm and the results on a case study are presented in section IV and discussed in section V.

II – Finite Element Method (FEM) modelling of a kite

II - 1 Principle of the method

To address the issues related to fluid structure interaction, a kite modelling based on the 3D scan of the *F-one Revolt* kite, i.e. on the inflatable tube structure shape at rest, was developed. The reconstructed shape of the kite is based on the three-dimensional geometry of the inflatable tube structure. The kite profile was identified on the kite inflatable batten 1 (figure 3) situated in the symmetry plane. The profile was considered to be constant along the span. Therefore, the 3D canopy shape was obtained by extending the symmetry plane profile along the span as presented in previous studies [5,6]. These assumptions were postulated in order to calculate the aerodynamic pressure load on the kite structure using the 3D lifting line coupled with XFOIL. Thus, the canopy shape is adapted to the CFD calculation method. Moreover, using a similar mesh, the aerodynamic load can be easily computed. The most common modelling of thin-membrane structure in Finite Element Method (FEM) is computed using membrane elements. The membrane elements are derived from the more commonly used shell elements. More advanced models were developed in order to better describe the fabric behaviour [7]. Trimarchi et al. [2] proposed an alternative method using a finite element shell model. Indeed, shell elements are commonly used to model structures in which one dimension, the thickness, is significantly smaller than the other dimensions. Like membrane elements, shell elements take into account the in-plane stress resultant, but they also take into account the bending stiffness of the material. The advantages of shell elements compared to membrane elements are:

- Shell elements are easier and faster to converge towards an equilibrium position.
- Reduction of wrinkles phenomenon within the canopy.
- In the long term, better modelling of the wrinkles size [2].

Shell elements also have disadvantages

- The bending stiffness must be defined. A sensitivity analysis was conducted in order to define the optimal bending stiffness to model the membrane behaviour of the fabric.
- Additional membrane stresses may appear due to non-zero bending stresses.

Shell elements were used to model the kite canopy with the following properties [7]:

- Membrane stiffness: $C = \frac{E_m \mu}{(1 - \nu^2)} = 624 .10^3$ N.m^{-1}
  - Weft specific Young modulus $E_m = 3510$ J.g^{-1};
  - Grammage (surface e density) μ: 170 g.m^{-2}
  - Poisson's ratio: $\nu = 0.206$
- Bending stiffness D defined by the ratio: $D/C = 10^{-6}$ m²

Beam elements were used for the kite LEI batten and inflatable battens 1, 2 and 3. LEI batten material characteristics are [7]:

- Grammage μ: 170 g.m^{-2}
- Warp specific Young modulus: $E_m = 2610$ J.g^{-1}
- Poisson's ratio: 0.094
- Thickness: 0.206 ± 0.002 mm (measured on the *F-one Revolt* fabric)

The radius of the leading edge inflatable tube and battens were measured on the 3D scanned *F-one Revolt* kite.

II - 2 Kite mesh generation

The fluid mesh was generated from a 2D profile mesh made with XFOIL. The 2D mesh was then extruded along the span to model the 3D geometry of the kite with the 3D lifting line. The LEI batten section which was entirely modelled in the 2D profile (in dashed line figure 1) was removed in the FEM modelling (in continuous line) as presented in figure 1 in the section j profile reference frame ($R_{p,j}$ ($\mathbf{x}_{p,j}$,$\mathbf{y}_{p,j}$,$\mathbf{z}_{p,j}$)) The FEM leading edge beam position was determined experimentally on the 3D scanned geometry of the kite.

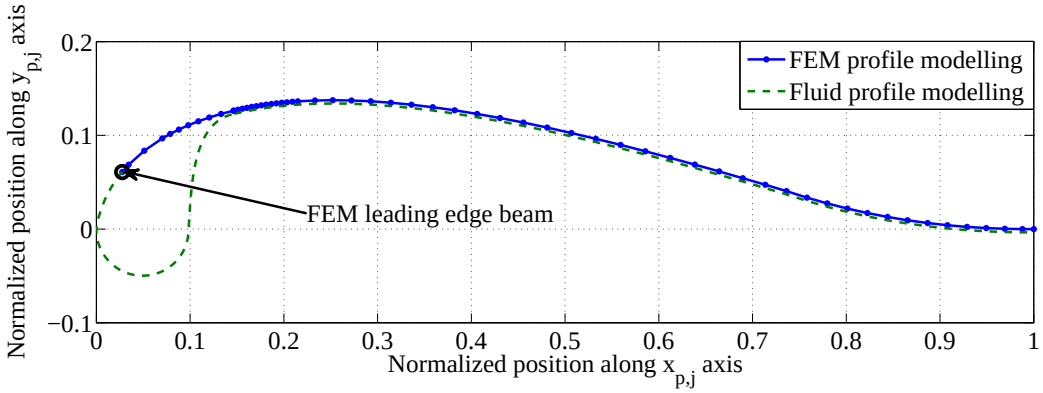

Figure 1. FEM and fluid profile modelling.

The position of a node along the chord was directly taken on the 2D FEM profile mesh as shown in figure 2. The position along the span corresponds to the position of the collocation points in the 3D lifting line calculation. Each node was referenced by its position along the span j and along the chord i as presented in figure 2 on the simplified unfolded kite. The canopy being modelled by quadrangle elements, element I,J was defined by 4 points: $S_{i,j}$, $S_{i,j+1}$, $S_{i+1,j+1}$, $S_{i+1,j}$.

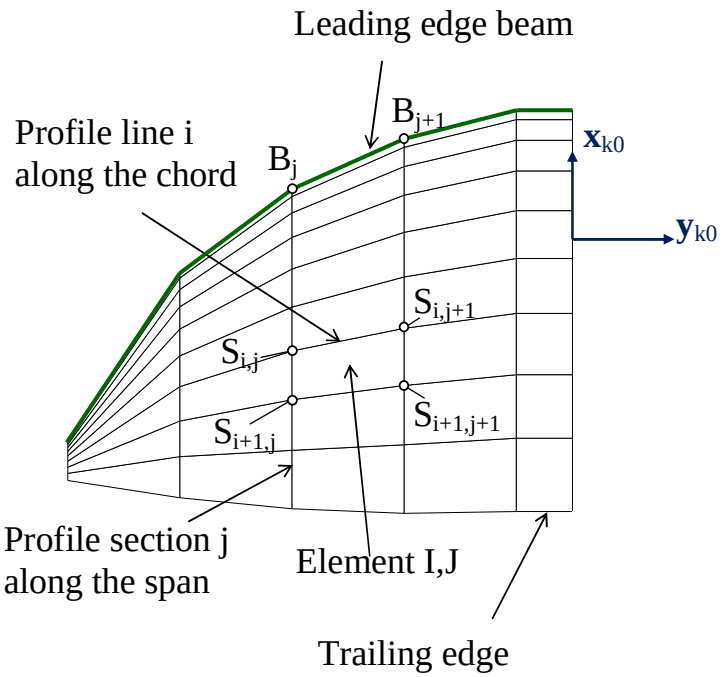

Figure 2. FEM mesh and pressure transfer on a half kite.

The LEI batten was modelled by beam elements (two nodes linear beam) as shown in figure 2. The beam element J was defined between points B_j and B_{j+1}. The inflatable battens 1, 2 and 3 were also modelled with beam elements as shown in figure 3. Each inflatable batten position was determined experimentally on the scanned kite. They were positioned on the canopy mesh along the corresponding profile.

II - 3 FEM kite boundary conditions

Only a half kite was modelled in the FEM solver as shown in figure 3. The nodes positions were defined in the R_{k0} (K,$\mathbf{x}_{k0}$,$\mathbf{y}_{k0}$,$\mathbf{z}_{k0}$) reference frame. A symmetry boundary condition was applied in the symmetry plane edge. The back lines were considered to be attached to the kite extremity at the leading edge. Therefore, the displacement of this node, called D in figure 3, along $\mathbf{z}_{k0}$ was null.

The two front lines were attached to the leading edge beam at nodes A1 and A2 as shown in figure 3. The positions of the attachment lines along the leading edge were identified on the 3D scan of the *F-one Revolt* kite. The forces exerted on the front lines are transmitted to a single front line through a pulley. To ensure the pulley equilibrium in the FEM modelling, a linear displacement equation or constraint can be defined in the FEM software. Therefore, $u_{A1,z}$ being the displacement of node A1 along $\mathbf{z}_{k0}$ axis, the displacement equation becomes

$$u_{A1,z} + u_{A2,z} = 2\, u_{P,z} \qquad (1)$$

Where $u_{P,z}$ is the displacement of node P along $\mathbf{z}_{k0}$ axis, node P being the pulley position. The position of node P has no influence on the results, but the displacement of node P must be equal to zero.

Finally, to ensure that the kite is not subject to rigid body motion along $\mathbf{x}_{k0}$, the simplest and fastest for the fluid structure interaction is to fix the displacements along $\mathbf{x}_{k0}$ of all kite nodes in order to divide the kite loads along $\mathbf{x}_{k0}$ axis within the whole kite.

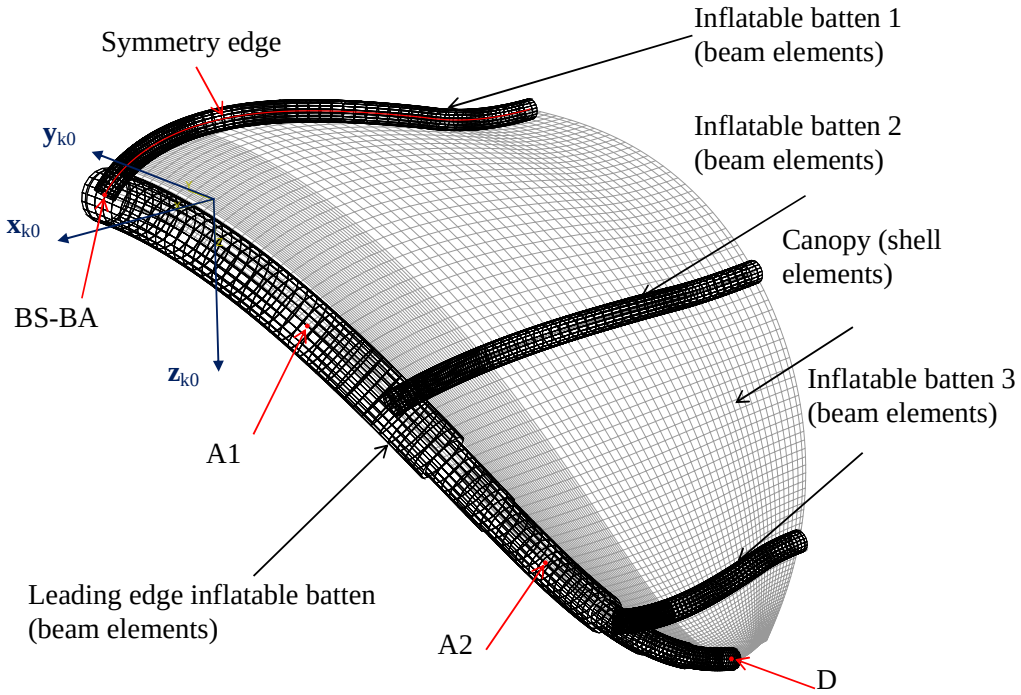

Figure 3. 3D kite FEM modelling based on the inflatable tube structure.

III – Load transfer from the 3D Lifting Line fluid calculations

The 3D lifting line presented in previous studies [5,6] was used for the pressure distribution identification within the kite structure. Only the leading and trailing edge node positions were needed for the 3D lifting line calculation. Indeed, in this method, the kite was divided in several profile sections. Each kite section was defined between a node on the leading edge and the corresponding node on the trailing edge. The bound vortices were arranged on the quarter chord along the span. The trailing vortices were disposed along the chord and then aligned with the incident flow. The collocation points were also disposed along the quarter chord line according to the horseshoe vortices distribution. The incidence of the kite was defined in the symmetry plane. The total lift and drag coefficients were calculated using the 3D lifting line. At the end of a fluid iteration, the apparent wind velocity $V_{a,j}$ and the effective incidence of each kite section $\alpha_{eff,j}$ were obtained. This allowed the pressure distribution along each profile section to be determined and transferred to the structure model of the kite.

III - 1 Aerodynamic pressure load distribution given by XFOIL

Each section profile was treated separately in order to transfer the pressure given by XFOIL to the FEM modelling. For each section profile, the 3D lifting line gave the effective incidence $\alpha_{eff,j}$ of a section. A lift coefficient C_L and a drag coefficient C_D correspond to the effective incidence $\alpha_{eff,j}$ of the profile section. To simplify the modelling, the profile was considered to be the same along the whole span as explained previously [5,6]. Therefore, the lift and drag coefficient evolutions as function of incidence are identical for all section profiles.

The pressure coefficient C_p distribution of the kite profile was calculated with XFOIL for all incidences between - 20 and 30 °. Therefore, knowing the incidence of a section

profile, the pressure coefficient distribution was interpolated from the data given by XFOIL as presented in figure 4.

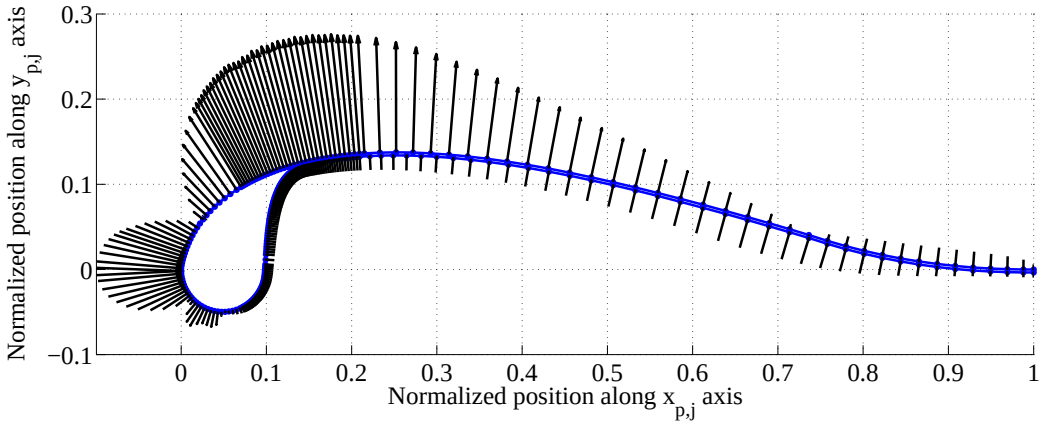

Figure 4. Pressure coefficient distribution along the kite fluid profile for an incidence of 4 °.

III - 2From fluid to FEM profile modelling

The profile used for the fluid modelling in XFOIL, shown in figure 4, is called fluid profile whereas the FEM profile modelling, shown in figure 5, is called FEM profile. In the FEM profile, the LEI batten was modelled by beam elements located at the intersection between the canopy and the LEI batten. The beam position was determined by the 3D scanned *F-one Revolt* kite. As presented in figure 5, the fabric or canopy, from the FEM leading edge to the trailing edge, was modelled by shell elements.

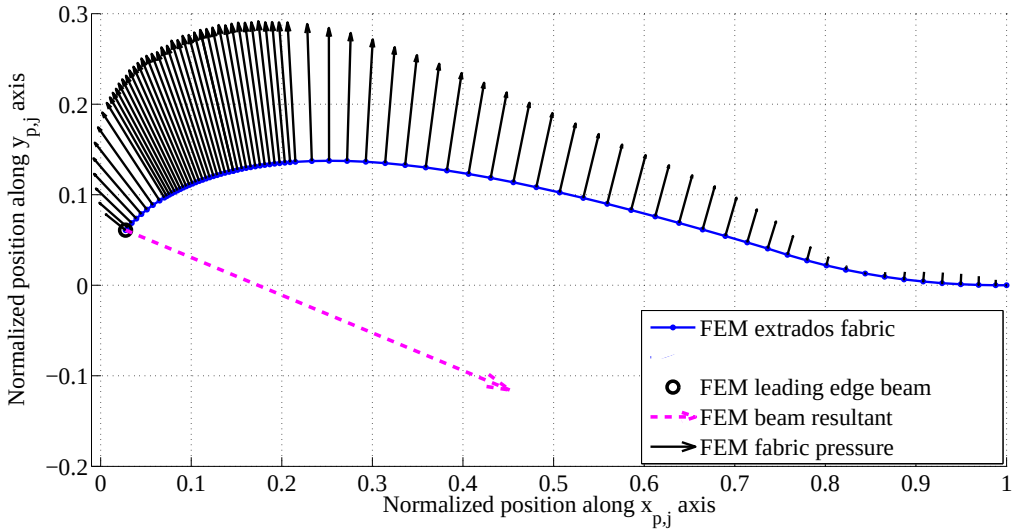

Figure 5. Kite FEM profile modelling and force transfer.

The FEM LEI batten was modelled by beam approach which is seen as a point in the section profile shown in figure 5. The kite profile for fluid analysis was divided into two parts: the fluid LEI tube and the fluid canopy (shown in figure 5).

III - 3 Pressure distribution transfer to kite FEM model

The pressure on the fluid extrados canopy in figure 4 was taken from XFOIL calculations on the fluid profile. At each point of the fluid extrados canopy, the fluid intrados

pressure was interpolated from the pressure distribution on the fluid intrados profile. As presented in figure 5, at each point of the FEM extrados canopy, the pressure is equal to the sum of the fluid profile extrados and intrados pressure shown in figure 4.

All the pressures in the fluid LEI batten part were transferred to the FEM leading edge beam. As presented in figure 5, the resultant pressure at each point of the fluid LEI batten is equal to the sum of the profile pressure and the inside pressure, considered to be constant in the fluid LEI batten. Then, the force at each point of the fluid LEI batten was obtained by multiplying the resultant pressure by the corresponding element size. The total force due to the fluid LEI batten was obtained by vectorial sum of all forces. The resultant moment was also calculated on the FEM leading edge beam.

The pressure on each profile element was obtained by multiplying the pressure coefficient C_p by ½ ρ_{air} $V_{a,j}^2$ ($V_{a,j}$ being the profile section apparent wind velocity and ρ_{air}) and transferred to the FEM model as presented in figure 5. The profile leading edge force was obtained by multiplying the FEM leading edge beam resultant by ½ ρ_{air} c_j $V_{a,j}^2$ (c_j being the chord of section j).

III - 4 Pressure and force transfer to the 3D geometry of the kite

The FEM mesh was directly taken from the fluid mesh as explained previously. The position of a node along the chord was directly taken on the 2D FEM profile mesh shown in figure 5. The kite canopy being modelled by quadrangle elements, element I,J is defined by 4 points: $S_{i,j}$, $S_{i,j+1}$, $S_{i+1,j+1}$, $S_{i+1,j}$. $P_{i,j}$ being the pressure calculated at point $S_{i,j}$, the pressure $P_{I,J}$ on element I,J is equal to:

$$P_{I,J} = \frac{P_{i,j} + P_{i,j+1} + P_{i+1,j+1} + P_{i+1,j}}{4} \quad (2)$$

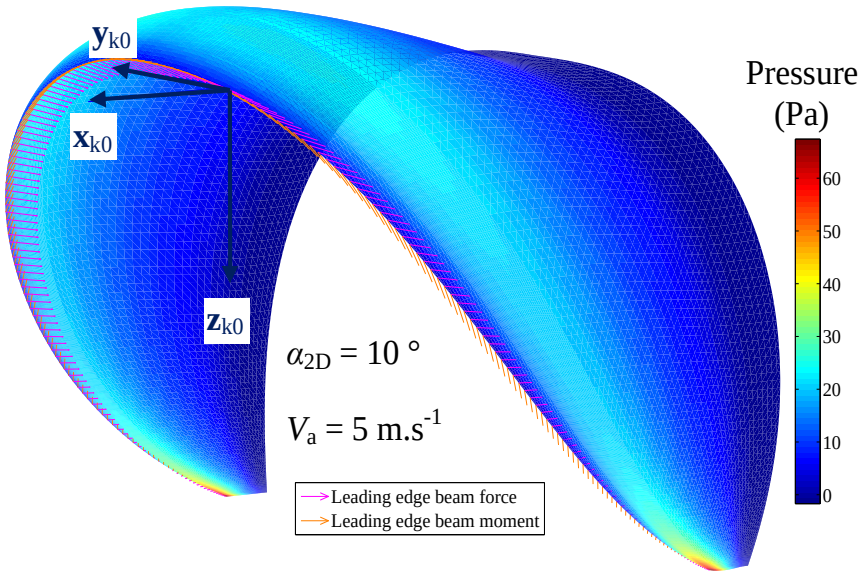

Figure 6. 3D FEM kite modelling and force transfer.

The leading edge beam force was applied at each beam node B_j. Its magnitude was obtained by multiplying the corresponding leading edge profile force by the half of the distance along the span between point B_{j-1} and point B_{j+1}. The two components of the leading edge beam force were expressed in the R_{k0} reference frame. The same operation was done

with the leading edge beam moment. The entire kite FEM loads modelling is shown in figure 6. The pressure on the canopy is plotted as well as the leading edge beam forces and moments.

IV – Fluid-Structure Interaction (FSI) and results

IV - 1 Fluid structure interaction loop

The global fluid structure interaction loop is presented in figure 7. At the beginning of a fluid calculation, the leading and trailing edge node positions resulting from the FEM calculation were given to the 3D lifting line. The apparent wind velocity was defined in the kite symmetry plane. It was reoriented at each fluid calculation in order to ensure that the kite incidence remains constant during the entire fluid structure interaction loop. Both section velocity and effective incidence were given to the load transfer routine. The fluid load was transferred to the FEM mesh in the load transfer module (figure 7) presented in section III. At the end of the 3D lifting line calculation, the aerodynamic resultant force $\mathbf{F}_a$ was obtained. This allowed the kite to be oriented so that $\mathbf{F}_a$ and $\mathbf{z}_{k0}$ are aligned, according to the assumptions of the zero-mass model [5,6]. The kite FEM mesh given at the beginning of the FSI loop was used as a reference for each FEM calculation. The initial node positions which were used in ABAQUS as a reference for the calculation of the stresses and strains in the elements was rotated at each iteration. Therefore, the initial FEM calculation geometry remains unchanged during all the fluid structure interaction process.

At the end of the FEM calculation, the loaded kite mesh position due to fluid loads was obtained. The leading and trailing edge node positions were extracted as presented in figure 7. This was re-injected at the beginning of the fluid structure interaction loop to initialize the fluid calculation.

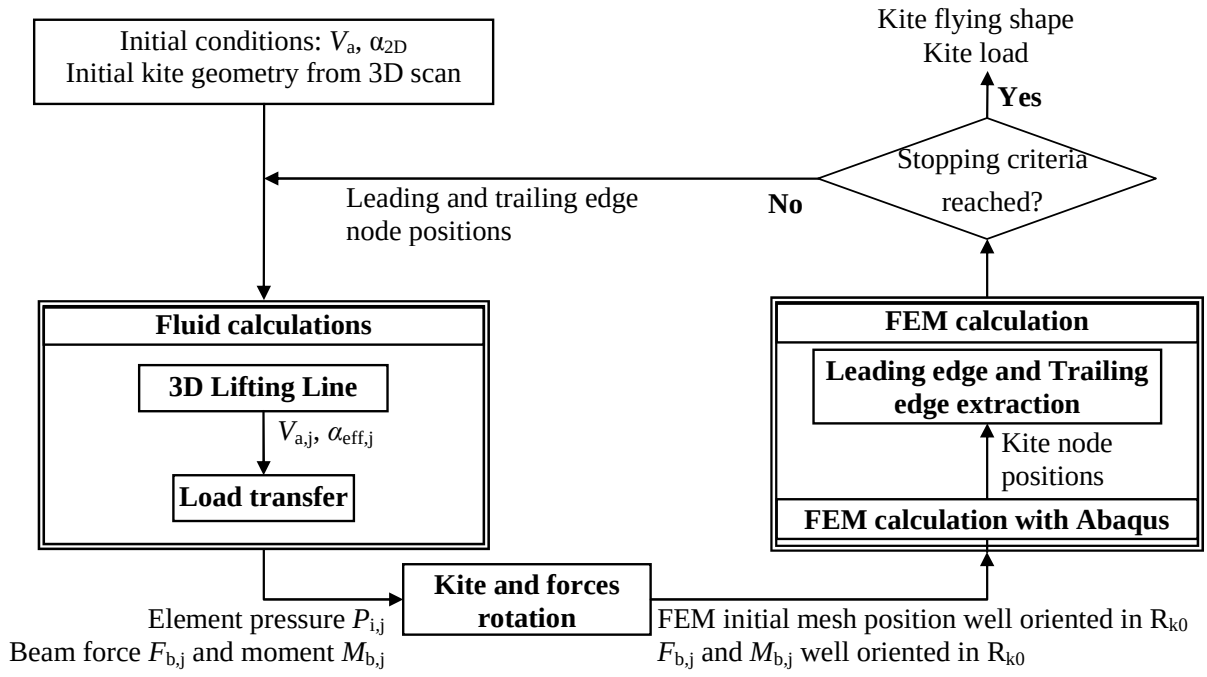

Figure 7. Fluid structure interaction loop scheme.

IV - 2 Fluid structure interaction results on a case study

The fluid structure interaction process was tested on a case study. The kite geometry was taken from the 3D scan of the kite at the beginning of the FSI process. The kite was

considered to be in static flight on the wind window edge. The apparent wind velocity in the symmetry plane of the kite, V_a, was equal to 5 m.s^{-1} and the kite incidence in the symmetry plane, α_{2D}, was 10 °.

To study the fluid calculation convergence, the norm of vector ($C_{p_{I,J}}^{k} - C_{p_{I,J}}^{k-1}$), called Σ_{Cp}^{k} was used, $C_{p_{I,J}}^{k}$ being the pressure coefficient C_p of element I,J at iteration k. To study the convergence of the FEM calculations, the norm of vector ($\mathbf{u}_{i,j}^{k} - \mathbf{u}_{i,j}^{k-1}$), called Σ_{u}^{k}, was used, $\mathbf{u}_{i,j}^{k}$ being the displacement vector of node ij between the initial and the equilibrium position of the FEM calculation at iteration k.

According to the Riemann criterion, if

$$\lim_{k \to \infty} k^{\alpha} \times \Sigma_{u}^{k} = 0 \text{ , and } \lim_{k \to \infty} k^{\alpha} \times \Sigma_{Cp}^{k} = 0, \text{ for } \alpha > 1 \tag{3}$$

Then, the series'

$$\sum_{p=1}^{p=k} \Sigma_{u}^{p} \text{ and } \sum_{p=1}^{p=k} \Sigma_{Cp}^{p} \tag{4}$$

converge. The vector series'

$$\sum_{p=1}^{p=k} \left(C_{p_{I,J}}^{p}\right) - \left(C_{p_{I,J}}^{p-1}\right) = \left(C_{p_{I,J}}^{k}\right) - \left(C_{p_{I,J}}^{0}\right) \text{ and } \sum_{p=1}^{p=k} \left(\mathbf{u}_{i,j}^{p}\right) - \left(\mathbf{u}_{i,j}^{p-1}\right) = \left(\mathbf{u}_{i,j}^{k}\right) - \left(\mathbf{u}_{i,j}^{0}\right) \tag{5}$$

converge, i.e., the sequences $\left(C_{p_{I,J}}^{k}\right)$ and $\left(\mathbf{u}_{i,j}^{k}\right)$ converge. If these two sequences converge, we can say that the fluid structure interaction process has converged. The fluid criterion ($k^{\alpha} \times \Sigma_{Cp}^{k}$, with α = 2) and FEM criterion ($k^{\alpha} \times \Sigma_{u}^{k}$, with α = 2) are plotted in figures 8 and 9. As shown in figure 8, the pressure coefficient criterion seems to converges towards zero along the FSI process. Therefore, one can say that the fluid structure interaction process converged according to the pressure coefficient criterion.

Figure 8. C_p criterion between two time steps as a function of number of iterations.

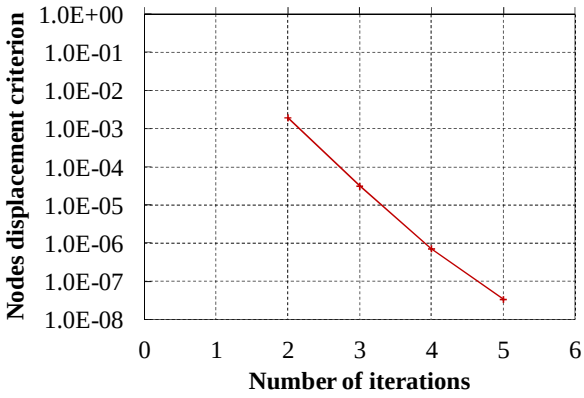

Figure 9. Node displacements criterion as a function of number of iterations.

The displacement criterion, displayed in figure 9 converges towards zero. As the pressure and displacement criteria converge towards zero, it can be concluded that the fluid structure interaction process converged. The FSI process was stopped after the 6th fluid iteration (and after the 5th structure iteration) since the fluid criterion is less than 10^{-6} (4.10^{-4} % of the C_p standard deviation) and the structure criterion is less than 10^{-9} m (1 nm = 10^{-9} % of the kite span).

The stress distribution was obtained within the kite fabric after each FSI loop. A fabric structure being bi-dimensional, the classical 3D invariants for the study of the stress and strain distribution cannot be used. Therefore, a bi-dimensional first invariant was defined as well as an equivalent to the Von Mises invariant. After the last iteration, the first stress invariant and the Von Mises equivalent invariant are plotted in figures 10 and 11. The specific stress field can be used for the kite fabric selection, since magnitude order of stress levels are consistent with the cylindrical shape analytic stress solution (pressure x radius / thickness). In this case, the mean cylindrical shape analytic specific stress is about 0.10 $J.g^{-1}$ for a radius R of 1 m and a grammage μ of 170 $g.m^{-2}$ and taking a mean pressure of 17.38 Pa.

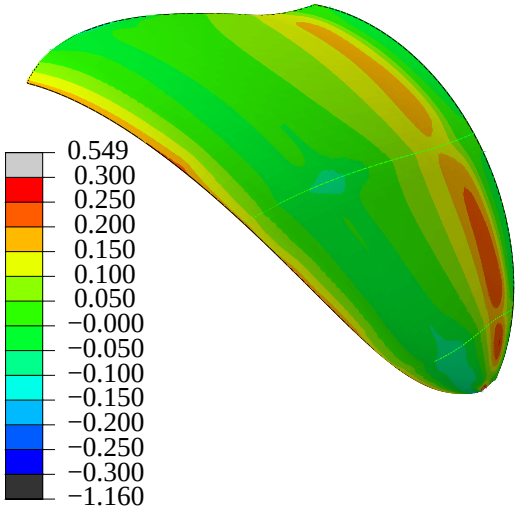

Figure 10. First stress invariant distribution after convergence of the FSI loop ($J.g^{-1}$).

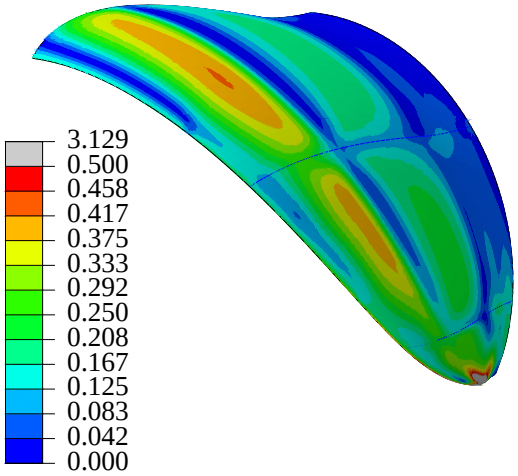

Figure 11. Second stress invariant distribution after convergence of the FSI loop ($J.g^{-1}$).

V – Discussion

Although computation time takes only several minutes for each iteration, in the future, it seems essential to automate the fluid structure interaction process. This implies that the ABAQUS FEM analysis must be launched automatically by Matlab® for example.

For the moment, the fluid structure interaction process was achieved by taking into account the initial position of the kite as a reference for the FEM calculations at each iteration. Therefore, the FEM calculation could be time consuming in more difficult cases since the final position could be far away from the initial position at each time step. The efficiency of the FEM calculations could be improved by starting an FEM calculation from the position at the end of the previous iteration. Nevertheless, this implies that the entire stress field at the end of the previous iteration must be taken into account as an input for each FEM calculation. This could improve the efficiency of the FSI process in the future.

The kite structure modelling would be improved in the future by taking into account the material properties by tensile test measurements on kite fabric samples. More refined material modelling characteristics would be used in the fluid structure interaction loop. In a second step, the non linear behaviour of the kite fabric can be taken into account with experimental data. The beam behaviour may also be adapted in order to take into account the inflatable battens buckling behaviour as was done by Breukels [4]. The fabric modelling can also be improved by taking into account the anisotropy of the kite fabric.

The fluid structure interaction method could be improved by applying more realistic loads and boundary conditions (taking into account the shear stress drag for instance). The method can also be applied to dynamic flight. Kite shape response to tether steering in turning stages could also be modelled in future works, namely to estimate possible aerodynamic characteristic modifications.

VI – Conclusion

The auxiliary propulsion of commercial ships requires huge kites that imply huge loads. Numerical tools must be implemented in order to design such kind of kite. The numerical modelling must take into account the kite structure deformation due to the aerodynamic load. Therefore, a Fluid Structure Interaction process was implemented.

The kite fluid modelling was done using the 3D lifting line method described in previous studies [5,6]. The flow around the kite was modelled using potential flow assumptions. The 3D lifting line method allowed us to take into account the three-dimensional flow effects which were not taken into account by Bosch et al. [1] in their fluid structure interaction process in . The viscosity was taken into account for each kite section using XFOIL. The load distribution, calculated by XFOIL for each section profile, was transferred to the profile structural modelling which comprises shell elements for the canopy and beam elements for the inflatable tubes structure. The pressure was transferred to the profile section fabric by summing the pressure on the extrados and intrados.

The fluid structure interaction was applied to a test case by considering a static flight. The information transfer between the fluid and structure calculations was done manually. After each iteration, the stress field within the canopy was obtained. It can be used for the kite fabric selection. Finally, the fluid structure interaction process allowed estimation of the stress level in the canopy. This will be very useful for the design of huge kites dedicated to auxiliary propulsion of commercial ships.

References

[1] A. Bosch, R. Schmehl, P. Tiso, D. Rixen: 'Nonlinear Aeroelasticity, Flight Dynamics and Control of a Flexible Membrane Traction Kite'. *Airborne Wind Energy. U. Ahrens, M. Diehl, R. Schmehl (eds.),* Springer, Heidelberg, ch 17. doi: 10.1007/978-3-642-39965-7_17.

[2] D. Trimarchi, M. Vidrascu, D. Taunton, D. Chapelle. 'Wrinkle development analysis in thin sail-like structures using MITC shell finite elements.' *Finite Elements in Analysis and Design,* 2013, vol. 64, p. 48-64. doi: 10.1016/j.finel.2012.09.005.

[3] V. Chapin, N. de Carlan, P. Heppel. 'A multidisciplinary computational framework for sailing yacht rig and sails design through viscous FSI'. *In: 20th Chesapeake Sailing Yacht Symposium,* Annapolis, USA, 2011.

[4] J. Breukels. 'An engineering methodology for kite design'. *Ph. D. Thesis, Delft University of Technology'*. 2011. http://www.kitepower.eu/publications.html

[5] R. Leloup, K. Roncin, G. Bles, J.-B.Leroux, C. Jochum, Y. Parlier. 'Estimation par la méthode de ligne portante de l'effet d'un virage sur la finesse : application aux cerfs-

volants de traction pour la propulsion auxiliaire des navires' *In: 13èmes Journées de l'Hydrodynamique*, Chatou, France, 2012.

http://website.ec-nantes.fr/actesjh/images/13JH/Articles/Leloup_JH13.pdf

[6] R. Leloup, K. Roncin, G. Bles, J.-B.Leroux, C. Jochum, Y. Parlier. 'Estimation of the lift-to-drag ratio using the lifting line method: application to a Leading Edge Inflatable kite', *Airborne Wind Energy. U. Ahrens, M. Diehl, R. Schmehl (eds.),* Springer, Heidelberg, 2013, ch. 19. doi: 10.1007/978-3-642-39965-7_19.

[7] W. Dib. 'Comportement mécanique de tissus à voile, en fibres synthétiques, sous sollicitations biaxiales et déformation finie (Mechanical constitutive law of a synthetic-fibre woven sailcloth, under biaxial loadings and finite strain)', *Ph.D. Thesis*, University of Grenoble, France, 2014.